

Photonic crystals for highly efficient silicon single junction solar cells

J. Krügener^{a,*}, M. Rienäcker^b, S. Schäfer^b, M. Sanchez^b, S. Wolter^b, R. Brendel^{b,c,d}, S. John^e, H.J. Osten^{a,c}, R. Peibst^{a,b}

^a Institute for Electronic Materials and Devices, Leibniz Universität Hannover, Schneiderberg 32, 30167, Hannover, Germany

^b Institute for Solar Energy Research Hamelin, Am Ohrberg 1, 31860, Emmerthal, Germany

^c Laboratory of Nano and Quantum Engineering, Leibniz University Hannover, Schneiderberg 39, 30167, Hannover, Germany

^d Institute of Solid State Physics, Leibniz University Hannover, Appelstrasse 2, 30167, Hannover, Germany

^e Department of Physics, University of Toronto, 60 St. George Street, ON M5S 1A7, Toronto, Canada

ARTICLE INFO

Keywords:

Photonic crystals
Silicon
Photolithography
Inverted pyramid texture
Surface passivation

ABSTRACT

The maximum achievable silicon single junction solar cell efficiency is limited by intrinsic recombination and by its limited capability of absorbing sun light. For Lambertian light trapping the maximum theoretical solar cell efficiency is around 29.5%. Recently a new approach for light trapping has been proposed for silicon photovoltaics. Highly regular structures with a size in the range of the wavelengths of the incident light act as so-called photonic crystals. Such structures allow wave-interference light trapping beyond the Lambertian limit. Applying these photonic crystals to silicon solar cells can help to reduce the absorber thickness and thus to minimizing the unavoidable intrinsic recombination. From a simulation study, we can conclude that 31.6% is the maximum possible single junction solar cell efficiency for a 15 μm -thin substrate. Furthermore, we present a process flow for the preparation of regular inverted pyramid structure, that acts as photonic crystal. Finally, regular inverted pyramid structures are prepared on polished and shiny-etched, i. e. on surfaces with a certain roughness, substrates. Surface passivation of these structured surfaces shows as good lifetimes as on conventional randomly pyramid textured surface. Excellent total saturation current densities on asymmetric samples of $4 \pm 2 \text{ fA/cm}^2$ for n-type and of $4.5 \pm 2.2 \text{ fA/cm}^2$ on p-type substrates are obtained.

1. Introduction

Neglecting minor differences in the decimal place, the photovoltaic community agrees that for Lambertian light trapping the maximum possible single junction silicon solar cell efficiency is around 29.5% [1–3]. For these theoretical calculations certain assumptions were made: single bandgap, no Shockley-Read-Hall recombination (bulk and surfaces), infinite carrier mobilities and perfect Lambertian light trapping. During recent years, a lot of effort has been taken to achieve the very limits for single junction silicon solar cells experimentally. The highest efficiencies reported so far are 26.7% for n-type [4] and 26.1% for p-type [5] silicon solar cells.

Recently, Bhattacharya and John proposed a new approach for silicon photovoltaics, which might allow a light trapping better than the Lambertian limit and would thus also allow for higher maximum possible solar cell efficiencies [6]. These authors proposed inverted pyramids with very small structure pitches to increase the absorption of the incident light. The use of inverted pyramids is apparently not a new

concept in silicon solar cells. The passivated emitter, rear locally-diffused (PERL) record efficiency solar cells from the University of New South Wales featured such a front side structure [7,8]. The major difference is found in the structures pitch of the inverted pyramids. Campbell and Green proposed structure pitches in the range of 10 μm [9]. Bhattacharya and John proposed much smaller pitches in the range of 1.3 μm –3.1 μm .

The dimensions of these regular structures are in the range of the incident wavelengths, especially for the longer ones for which light trapping matters most. This combination leads to the formation of a so-called photonic band structure. The reason for an increased absorption under certain circumstances is based on two effects. The first effect is parallel to interface refraction, where the light moves parallel to the refraction plane after refraction [6,10]. This leads to group velocities parallel to the interface and therefore to a different propagation of the light. Second, the group velocities are strongly reduced. These so called slow light modes result in a higher absorption probability due to higher „dwell time“ at a given position. Such photonic crystals (PCs) aren't a

* Corresponding author.

E-mail address: kruegener@mbe.uni-hannover.de (J. Krügener).

<https://doi.org/10.1016/j.solmat.2021.111337>

Received 13 May 2021; Received in revised form 29 July 2021; Accepted 13 August 2021

Available online 20 September 2021

0927-0248/© 2021 Elsevier B.V. All rights reserved.

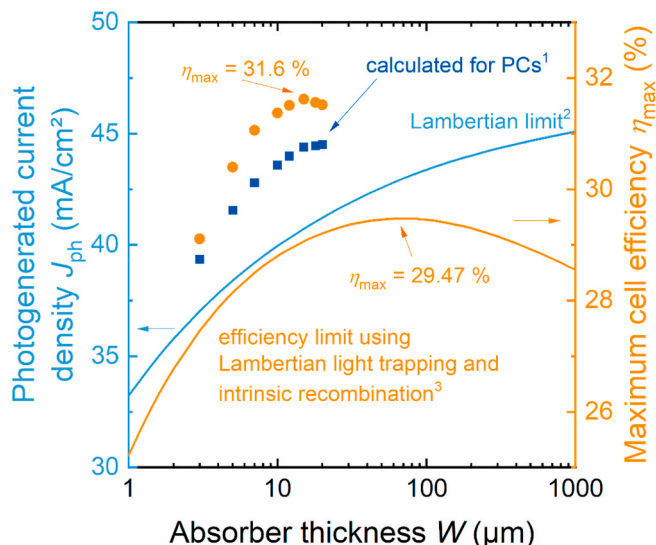


Fig. 1. Calculated photogenerated current density as function of the Si absorber thickness in light blue, following the Lambertian limit [3]. In orange the maximum possible calculated Si solar cell efficiency is shown, using the data in light blue and intrinsic recombination [1]. The full blue squares correspond to calculated photogeneration current densities from Ref. [18]. The full orange circles represent the corresponding maximum calculated Si solar cell efficiencies. All calculations neglect surface and Shockley-Read-Hall recombination. (For interpretation of the references to colour in this figure legend, the reader is referred to the Web version of this article.)

man-made concept and are often found in the nature. For example, the shimmering colors of butterfly wings are a result of such periodic structures, e. g. Refs. [11,12]. In the late 1980s Yablonovitch [13] and John [14] proposed to use similar, but artificially prepared, structures for technical applications.

First experimental proof of light trapping above the Lambertian limit using photonic crystals in silicon was recently reported by Hsieh et al. [15]. Hsieh et al. prepare periodic inverted pyramids and so-called teepee structures on 10 μm thin silicon on insulator substrates by electron beam lithography (EBL) and deep UV photolithography, respectively. For these structures a higher absorption, for wavelengths above 900 nm compared to the Lambertian limit was reported. The corresponding calculated photogeneration current densities are 41.29 mA/cm² for the inverted pyramids and even 41.52 mA/cm² for the teepee structures compared to 39.63 mA/cm² for Lambertian light trapping [15]. The higher absorption potentially allows a reduction of

the absorber thickness and thus reduces the overall intrinsic recombination.

In this paper two main topics will be discussed. First we will give a calculation of the maximum achievable efficiency for a single junction solar cell when using photonic crystals instead of conventional light trapping schemes. Second we will present an approach for the preparation of photonic crystals in silicon using conventional i-line photolithography instead of electron beam and deep UV lithography. Here, we present a process flow for the preparation of inverted pyramids with structure pitches in the range of 1.9 μm and 3.1 μm. Finally, regular inverted pyramid structures are prepared on polished and shiny-etched, i. e. on surfaces with a certain roughness, substrates. All samples are characterized in terms of structural transfer, e. g. homogeneity, potential surface passivation and current status of optical characterization.

2. Intrinsic efficiency potential of silicon solar cells with photonic crystals

In the first section of this paper, we give a calculation of the intrinsic efficiency potential with photonic crystals in silicon photovoltaics. For all results shown in the following, we considered only intrinsic recombination using the analytic parametrization from Veith-Wolf et al. [1] for n-type silicon. Extrinsic losses due to Shockley-Read-Hall recombination and resistive losses are neglected. The Lambertian efficiency limit, also known as the Yablonovitch limit [16], is calculated using the recent approach by Schäfer and Brendel [3] that accounts for the reabsorption of radiatively emitted photons.

First, we use the well-known relation of the photogenerated current density as a function of the silicon absorber thickness as shown in Fig. 1. Here, the photogenerated current densities are calculated assuming Lambertian light trapping [3]. The light blue curve in Fig. 1 shows the resulting photogeneration current densities. We calculate the maximum achievable silicon solar cell efficiency for a cell limited by intrinsic recombination [1]. All losses at the surfaces and contacts are neglected. The maximum of this curve is about 29.47% at a thickness of around 80 μm in agreement with [1].

Now we use the photogenerated current densities as calculated by Bhattaraya and John for PCs with absorber thicknesses between 3 μm and 20 μm for normal incidence [17]. These values are shown in Fig. 1 as blue squares. A larger current is simulated for the PCs than for perfect Lambertian light trapping. Next, we use these higher photogenerated current densities to calculate the maximum achievable silicon solar cell efficiencies, again using only intrinsic recombination. The results of these calculations are shown as orange circles in Fig. 1. The maximum cell efficiency is 31.6% for a 15 μm-thin silicon absorber. This value is around 2% points higher than the Lambertian efficiency limit for silicon

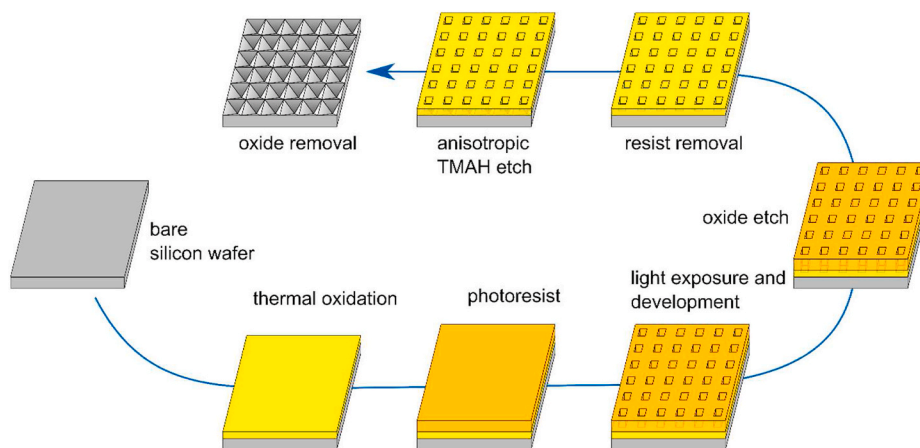


Fig. 2. Process flow for the preparation of inverted pyramids for use as photonic crystals in silicon. (For interpretation of the references to colour in this figure legend, the reader is referred to the Web version of this article.)

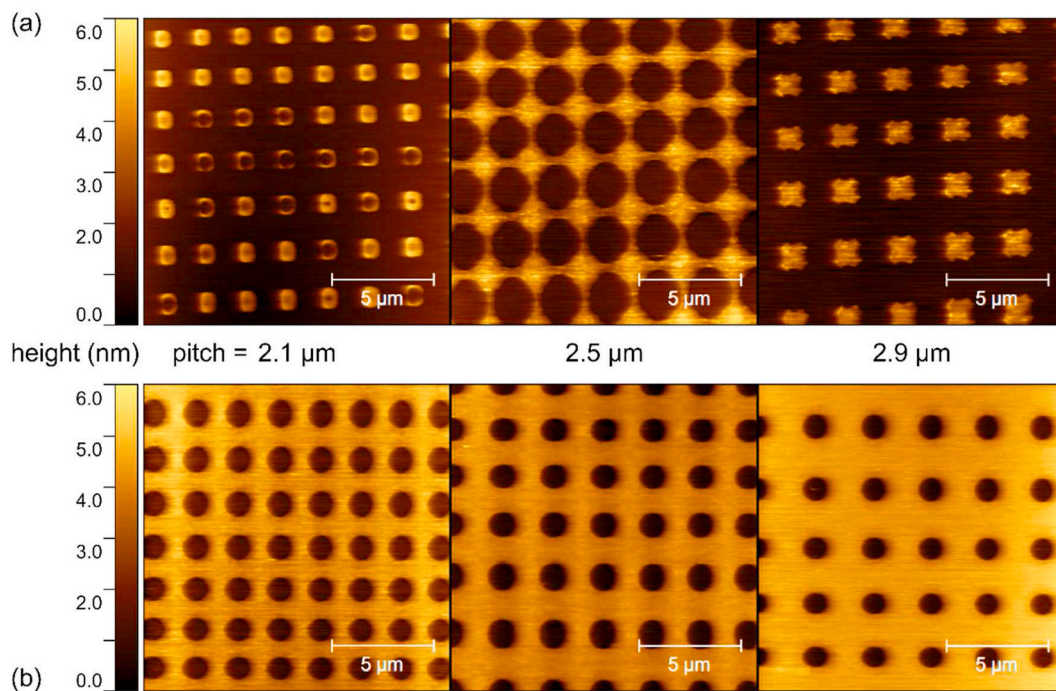


Fig. 3. AFM images of an initially 6 nm thin silicon oxide layer after structuring with diluted hydrofluoric acid through a resist mask. The images in (a) represent non-ideal conditions in terms of the structural transfer of the initially desired patterns. The images in (b) represent ideal pattern transfer. (For interpretation of the references to colour in this figure legend, the reader is referred to the Web version of this article.)

single junction solar cells. Furthermore, the optimum absorber thickness, i. e. for a maximum solar cell efficiency, reduces from around 80 μm down to 15 μm .

The reason for this difference is the increased light absorption of silicon absorbers using PCs compared to conventional Lambertian light trapping. Much thinner absorbers reduce the intrinsic recombination losses and thus increase the maximum achievable efficiency.

3. Experimental preparation of photonic crystals

3.1. Process flow for preparation of photonic crystals using photolithography

We prepare periodic inverted pyramid structures by photolithography in combination with anisotropic etching. Fig. 2 sketches our process flow. We apply structural pitches in the range of 1.9 μm –3.1 μm . A thin silicon oxide (~4–6 nm) layer is thermally grown on a bare silicon wafer. This oxide layer acts as a mask for the latter anisotropic etching step. We found that this hard mask is required since the resist does not withstand the anisotropic etching step. The silicon oxide hard mask is structured by a locally structured photoresist (AZ1505), using diluted hydrofluoric acid (2%, 30 s). The pattern on the photolithography mask consists of squares with dimensions of 0.75 μm and 1 μm , respectively. The transferred pattern consists of a regular hole pattern with circular hole openings, due to diffraction at the corners of the structures. The small feature size together with the small pitch periodicity of the desired structures are at the very resolution limit of the used i-line (wavelength of 365 nm) photolithography (Karl Suss MA-150). The photoresist is then removed (remover AZ100) before anisotropic etching. Next, the structured silicon oxide layer acts as a hard mask for the silicon with tetramethylammonium hydroxide (TMAH) at 70 °C. We use diluted TMAH solution (7.5%) and etching durations between 9 min and 11 min, depending on the structural pitch. The silicon oxide layer is not etched due to the high selectivity between silicon and the masking oxide layer around 7000:1 for Si(001) planes of TMAH at 70 °C [18–20]. For optimized lithography and etching conditions, we observe a regular

matrix of inverted pyramids as shown in section 3.3.

Photolithography is not a viable technique for the industrial production of photovoltaic cells. However, it is a versatile and flexible technique in the lab for a proof of concept. Conventional photolithography - other than electron beam lithography [15] - is a simple method to prepare photonic crystals on a large area and even on non-polished, e. g. shiny-etched, surfaces. This, way the optical performance of PCs on hilly surfaces can be characterized, which would be challenging to describe by rigid Maxwell equation simulations. Provided that the photonic crystals demonstrate the expected advantages also on rough surfaces, the next step for industrialization could be the development of a photolithography-free preparation process, e. g. by laser interference and imprint [21,22].

3.2. Pattern transfer from resist to oxide etch mask

Initial attempts to use the photoresist as an etching mask failed, due to delamination of the resist in the etching process. Therefore, we chose to use a thermally grown silicon oxide layer as a hard mask for the anisotropic etching process step. The etch rates between the silicon and the silicon oxide differ by a few orders of magnitude [18]. Thus a few nanometres of silicon oxide layer are sufficient for masking the etching process of inverted pyramids with dimensions as desired here.

However, the pattern transfer from the resist into the silicon oxide layer is challenging. We use atomic force microscopy (AFM) to characterize the pattern transfer from the resist into the oxide layer. AFM allows a high lateral and height resolution, as required for the intended 4–6 nm deep holes. For non-ideal conditions, we find different kinds of defective pattern transfer as shown in Fig. 3a. The figure shows exemplarily three different types of commonly observed defective reproduction of the initial pattern. In the left picture of Fig. 3a, the structures are over-developed. Thus the rims between the holes are removed too during resist development. The image in the middle of figure Fig. 3a is an example for an over-etched structure, i. e. with a too small rim around the intended hole, whereas the rightmost image is a mixture of both aforementioned non-idealities.

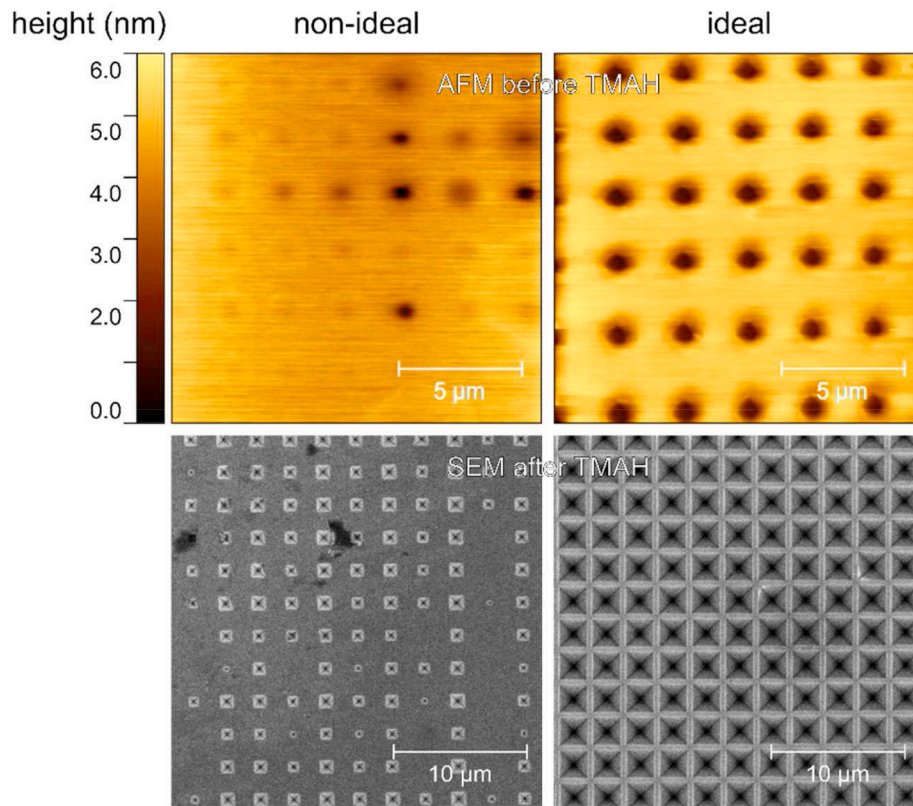


Fig. 4. (top) AFM images of etched silicon oxide masking layer for non-ideal left and ideal transferred patterns. (bottom) the corresponding SEM images after anisotropic TMAH etching.

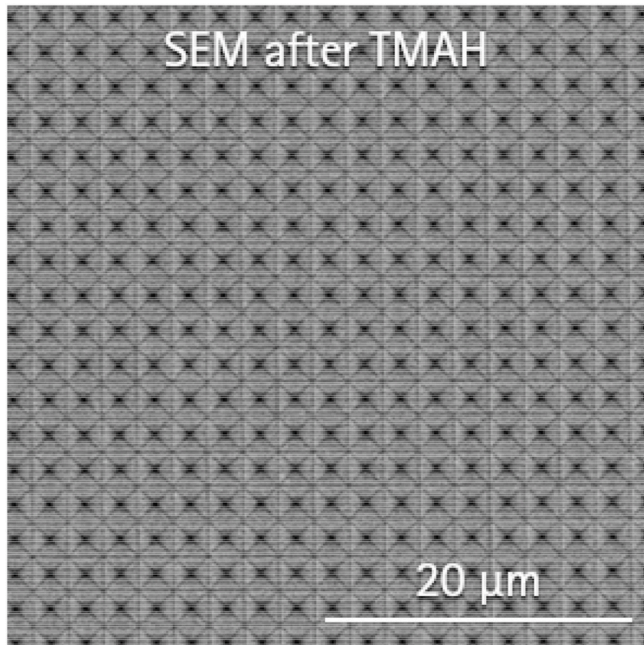


Fig. 5. SEM image of a silicon surface after masked anisotropic etching with TMAH. The structure pitch of this structure is 2.3 μm .

In Fig. 3b AFM images after oxide structuring under more ideal conditions are shown. In comparison to Fig. 3a we observe a regular pattern transfer into the oxide layer. Instead of the square openings in the lithographic mask, we find circular ones due to diffraction at the structure corners.

3.3. Anisotropic etching of inverted pyramids

In the next step, we use an anisotropic TMAH etch to transfer the pattern from the silicon oxide mask onto the silicon substrate. As shown in the previous section, the quality of the openings in the oxide hard mask is a very important parameter for the anisotropic etching process. In Fig. 4 one example for non-ideal and one for ideal pattern transfer are presented. The images on the top are AFM images taken after oxide structuring, i. e. after structuring the silicon oxide masking layer with DHF. The AFM image of the non-ideal case shows a very inhomogeneous distribution of the etched holes as well as differing etch depths of the latter. After TMAH etching of such a structure, we observe, as expected, an inhomogeneous distribution of inverted pyramids as shown in the SEM image on the lower left of Fig. 4. On the other hand, a regular and homogeneous pattern transfer from the photoresist into the silicon oxide hard mask (Fig. 4 top right) results in regular and homogeneous structures after anisotropic etching (Fig. 4 lower right).

Please note that the wide ridges between the inverted pyramids result from a non-optimized TMAH etching process. A further optimization of the etching conditions, results in surface structures like shown in Fig. 5. Here, the process flow results in a regular arrangement of inverted pyramids with very small ridges in-between. In the example shown in Fig. 5, the ridge width is slightly below 150 nm. However, for high quality photonic crystals a further reduction of the ridge width is needed as already mentioned by Hsieh et al. [15].

In contrast to the pattern transfer into the oxide mask, the conditions of the anisotropic etching step seem not to be crucial parameters. Aside from the structure pitch of the inverted pyramids, only the presence of a native oxide layer within the hole pattern, impacts the etching duration. If a native oxide is grown within the holes of the oxide layer mask, e. g. due to delay in the processing sequence, the anisotropic etching step needs much longer compared to a freshly prepared sample without such an oxide.

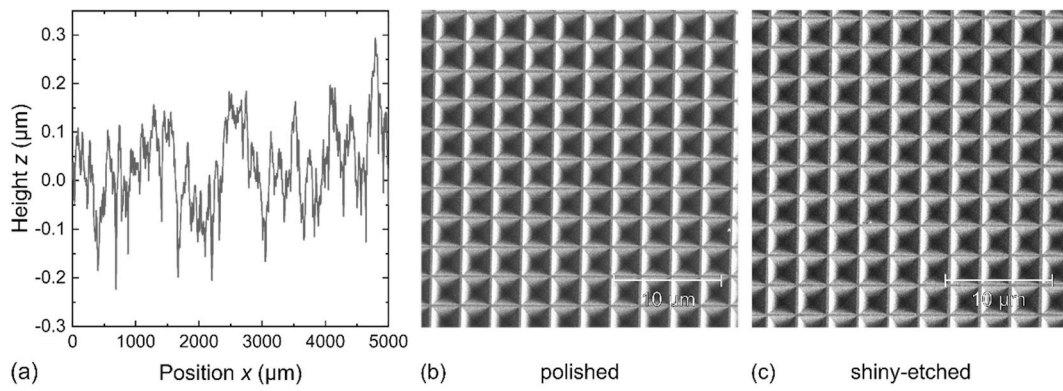


Fig. 6. (a) Height profile of a shiny-etched silicon surface. SEM after masked anisotropic etching of (b) an initially polished and (c) of an initially shiny-etched surface. The structure pitch is 2.7 μm. (For interpretation of the references to colour in this figure legend, the reader is referred to the Web version of this article.)

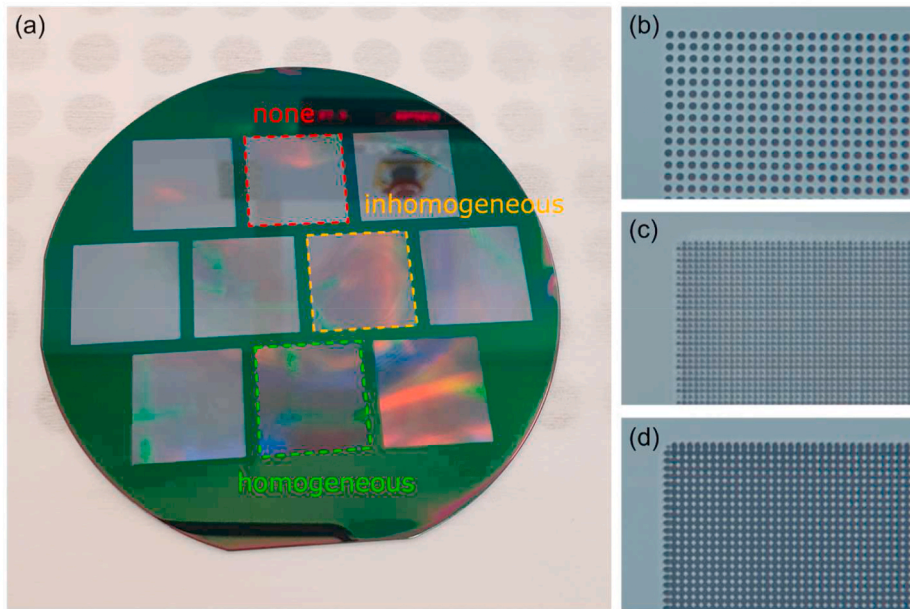


Fig. 7. Optical images of a wafer with developed resist. (a) Three types of structures can be observed: none (red), inhomogeneous distributed (orange) and homogeneous (green). (b) Good pattern transfer to the developed resist. (c) Defective pattern transfer to the resist due to interference within the structures. (d) Overexposed structures with only small mesa-like structures left. (For interpretation of the references to colour in this figure legend, the reader is referred to the Web version of this article.)

3.4. Impact of the initial surface morphology

All structures presented so far are prepared on polished surfaces. However, in silicon solar cells, even in lab-scale ones, commonly damaged-etched or shiny-etched substrates are used. Damage-etched or shiny-etched surfaces exhibit a surface roughness in the range of a few micrometres. In Fig. 6a a height profile, measured with a Dektak profilometer, of a shiny-etched silicon surface is shown. For such uneven surfaces, the use of conventional photolithography, might be much more suitable than EBL structuring of the etching mask. The latter techniques need a perfect focusing of the electron beam at the substrate surface. Thus, a certain roughness might lead to a defocused structure transfer or even to no transfer. This issue is avoided by using conventional photolithography allowing a direct comparison of the optical properties of initially polished and uneven surfaces. However, photolithography will remain a technique used in research rather than for industrial applications. For the latter eventually a process based on laser interference or something similar fast has to be developed - in case the use of PCs offers practical benefits for silicon solar cells.

In Fig. 6b and c SEM images of regular inverted pyramid structures with a structure pitch of 2.7 μm are shown. The structures in (b) are prepared on an initially polished surface, whereas in (c) on an initially shiny-etched surface. Both structures are of the same quality and we see

no differences. The transfer of this process onto damage-etched samples, as well as the characterization of the optical modes formed by PCs on uneven surfaces, is currently ongoing.

3.5. Homogeneity issues

The small feature size of the desired structures in combination with the used light with a wavelength of 365 nm (i-line) leads to some unwanted effects. First of all, the transferred pattern into the resist and thus the oxide layer does not consist of squares, as they are present on the lithographic mask, see for example Fig. 3. This rounding of the structures is simply caused by diffraction of the light at the corners of the structures.

Fig. 7a shows a photograph and light microscopic images. We observe inhomogeneities across the wafer. The field marked in red did not develop a pattern. The field in orange shows an inhomogeneous pattern. And finally the field in green has a homogeneous pattern. The presence of the regular structures is indicated by the colors gradient in the different regions. This issue arises from the initially mentioned combination of the used light, the small structure size (~1 μm) and the regular arrangement of the structures.

Fig. 7b shows the case for a good pattern within the resist. Such a structure allows a regular and homogeneous pattern transfer to the

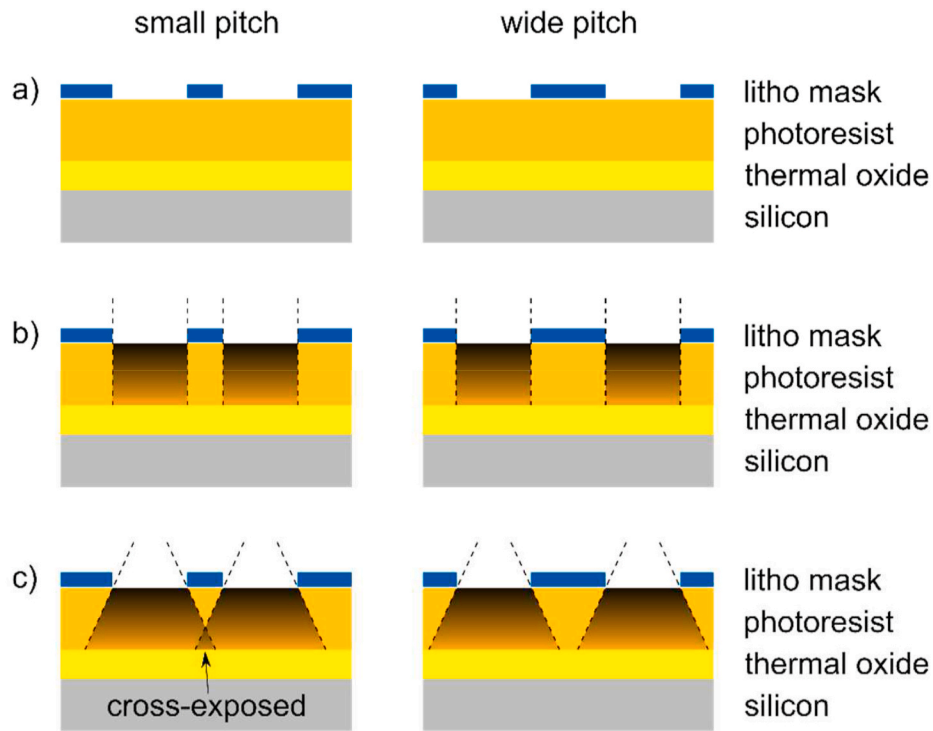


Fig. 8. Schematic cross section with (a) resist before light exposure. (b) Light propagation during exposure for perfectly collimated and (c) with a certain divergence of the incident light.

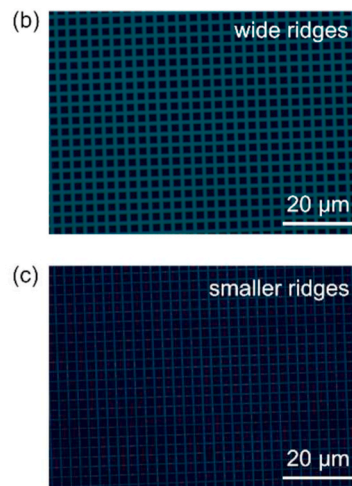
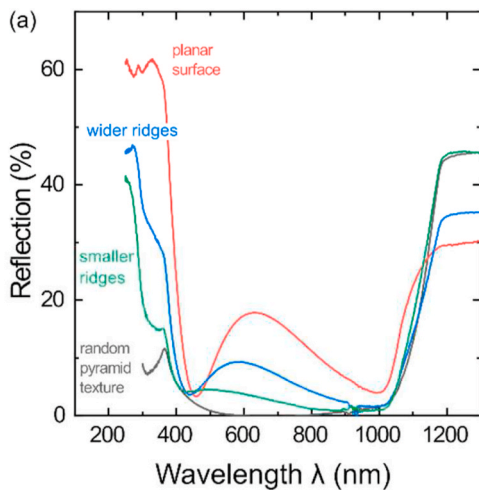


Fig. 9. (a) Reflection data of different photonic crystal structures with wider (blue) and smaller (green) ridges in-between the inverted pyramids. Reflection data of planar (red) and randomly textured (grey) surfaces act as references. Optical microscopic images of the corresponding structures with (b) wider and (c) smaller ridges. The regular structures are prepared on p-type substrates with a resistivity of 1.3 Ohm cm and a thickness of 280 μm. (For interpretation of the references to colour in this figure legend, the reader is referred to the Web version of this article.)

underlying oxide layer, e. g. as shown in Fig. 3b. Fig. 7c corresponds to a case where the resist gets cross exposed in some regions. In Fig. 8a, a schematic sketch of structures consisting of thermal oxide with photoresist on top and the photolithographic mask above is sketched. Fig. 8b gives the corresponding light propagation during light exposure in case of a perfect collimated light beam. All structures can be assumed to be transferred perfectly into the resist. In case of a divergent light beam, the case shown in Fig. 8c might be observed. For structures with a small pitch, light from adjacent openings in the mask might reach undesired regions. The combined light intensity can be high enough to make it solvable in developer solution. This way structures like shown in Fig. 7c can be explained. If the cross exposure or the overall light intensity is too high, one can observe defective structures like shown in Fig. 7d.

From these results, we can conclude that the combination of used light source and structures pitches make it necessary to optimize the

preparation process for each structure.

4. Optical characterization and passivation of photonic crystals

4.1. Optical characterization of regular inverted pyramid structures

For optical characterization, we prepare regular inverted pyramid structures on polished p-type (1.3 Ohm cm) substrates with a thickness of 280 μm. Before optical characterization, all sample surfaces are passivated with a 20 nm thin AlO_x, deposited by atomic layer deposition. The front sides with the regular inverted pyramid structures are passivated with a triple passivation and anti-reflection layer stack. This stack consists of 20 nm AlO_x followed by 54 nm plasma-enhanced chemical vapour deposited (PECVD) SiN_y layer with a refractive index of 1.9. Finally, 120 nm PECVD SiO₂ are deposited on top. These

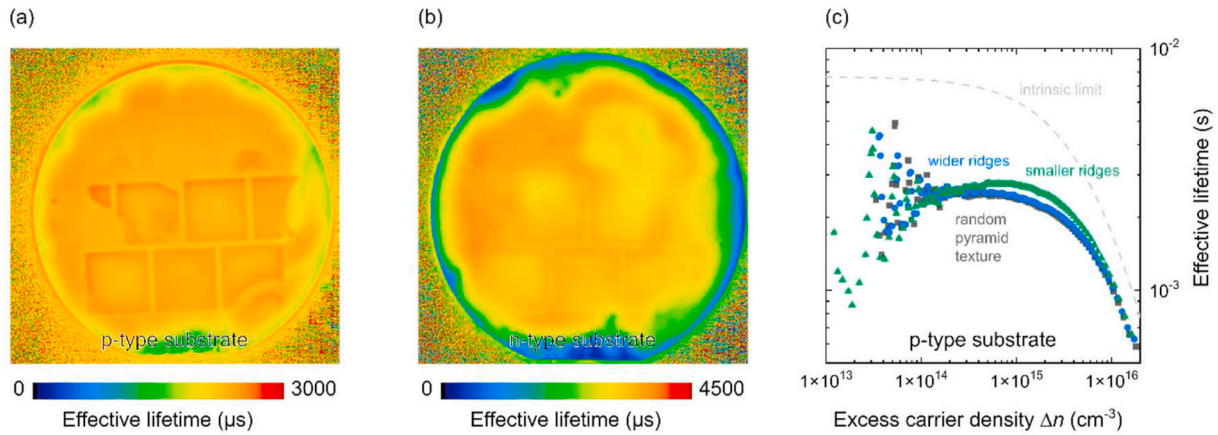


Fig. 10. Infrared Lifetime Mapping images of samples with periodic inverted pyramids in (a) p-type and (b) n-type substrates. (c) Photoconductance decay measurements of structures shown in Fig. 9 (b) in blue and (c) in green. Measured lifetimes of a randomly pyramid textured are shown as reference. The lifetimes in (c) are measured on p-type substrates. (For interpretation of the references to colour in this figure legend, the reader is referred to the Web version of this article.)

thicknesses are measured when the deposition is on planar samples. Please note that these layer thicknesses are optimized for random pyramid textured surfaces and not for inverted pyramid structures.

We measure the hemispherical reflection of the inverted pyramid structures using an integrating sphere. Here, the specular reflectance and the diffuse part of the reflected light are measured. Fig. 9 summarizes the reflection data of two passivated PC structures together with planar and random pyramid textured references. A direct comparison of those two references demonstrates the higher reflection of the planar sample, especially for wavelengths below 400 nm and around 630 nm (see red curve in Fig. 9a). The regular inverted pyramid structures, we prepared so far, show a reflection behaviour which is situated in-between the reference samples. Decreasing the ridge width between the inverted pyramids, comes in hand with a reduction in reflectance of the surface. Especially the reflection hump around medium wavelengths (peak around 630 nm) of the planar surface, reduces with further reduction of the ridge width. Here, the non-optimized anti-reflection coating on the planar regions, plays a significant role, leading to the observed hump in the medium wavelength of the reflection data. The impact of the ridges for the overall reflectance is already visible with an optical microscope. Fig. 9b and c shows the optical microscopic images corresponding to the reflection data in Fig. 9a. The ridges are bright whereas the inverted pyramids are nearly black.

At this point the high reflection of our regular inverted pyramid structures does not allow an increased absorption with respect to the random pyramid structure. Therefore, measurements of the absorption are not discussed here.

The above shown results show that the ridge width between the inverted pyramids has to be reduced. At the moment, the minimum ridge width is about 150 nm. As Hsieh et al. pointed out, this value is the crucial parameter and needs to be reduced to a few 10th of nanometres [15]. Here, the anisotropic etching step is the critical point to control the ridge width. For such structures absorption and angle-resolved reflection measurements are planned.

4.2. Surface passivation of regular inverted pyramids

In this section, first results of surface passivation of regular inverted pyramid structures will be discussed. All structures are asymmetrically passivated by the same layers as mentioned in the previous section: 20 nm ALD AlO_x on the rear and 20 nm AlO_x/54 nm SiN_y/120 nm SiO_z on the front side. The reason for this asymmetrical passivation scheme originates from the final solar cell structure we are aiming for, i. e. for an interdigitated back-contacted polycrystalline silicon on oxide (POLO) cell [5,23,24]. In Fig. 10 Infrared lifetime mapping (ILM) images of

p-type (1.3 Ohm cm) and n-type (20 Ohm cm) are shown [25,26]. Here, the local structural inhomogeneities of the different pitches (see section 3.5) are again apparent. Aside from these effects, both samples demonstrate high effective carrier lifetimes and lifetime homogeneities within the structured regions.

Next, local photoconductance decay (PCD) measurements are performed on 2 × 2 cm² regions of the same samples discussed in section 4.1 [27]. Fig. 10c shows corresponding measured effective lifetimes as a function of the excess carrier density. The measured characteristics of the random pyramid textured front surface and the one with wider ridges between the inverted pyramids (see Fig. 9b) are nearly identical. The sample with smaller ridges (see Fig. 9c) shows a very similar characteristic, but with slightly higher lifetimes at excess carrier densities around 10¹⁵ cm⁻³. A possible explanation of this apparent benefit of the inverted pyramids, could be the regular structure of the inverted pyramids compared to the randomly pyramid textured surfaces. For the latter, re-entrant ridges or edges can often be found. These regions might be harder to passivate or have a different passivation quality, e. g. due to a higher density of interface defects. However, the uncertainty of the PCD measurements is usually higher than the measured difference here. Thus we can conclude that the passivation of the regular inverted pyramids works at least as good as one random pyramid textured surfaces.

The asymmetric sample structure does not allow the determination of the single-sided saturation current density after Kane and Swanson [27], but a total one. Here, a value of 4 ± 2 fA/cm² for n-type (20 Ohm cm) samples and of 4.5 ± 2.2 fA/cm² for the samples shown in Fig. 10c can be extracted.

5. Conclusion

In this work, we simulate the maximum efficiency of single junction silicon solar cells limited by intrinsic recombination and featuring regular inverted pyramids with structure pitches in the range of 1.9 μm–3.1 μm under normal incidence. For this we use calculated photocurrent densities by Bhattacharya and John [17] together with state-of-the-art intrinsic recombination models. In doing so, we are able to show that the maximum efficiency achievable is around 31.6% and exceeds the limit of 29.5% for Lambertian lighttrapping. The larger efficiency limit is a result of an absorber thickness that can be reduced down to 15 μm due to the improved optical absorption. Furthermore, we present a process flow for the preparation of regular inverted pyramids using conventional i-line photolithography. All our samples were characterized in terms of structural homogeneity, surface passivation and reflectance. Issues with lacking structural homogeneity of the transferred patterns as well as further optimization in terms of optical properties are subject of ongoing

work.

Finally, regular inverted pyramid structures are prepared on polished and shiny-etched, i. e. on surfaces with a certain roughness, substrates. The surface passivation of asymmetric samples, i. e. structured front side and planar rear side, show as high lifetimes as those measured on a conventional random pyramid textured surfaces. Total saturation current densities (sum for both surfaces) on asymmetric samples of $4 \pm 2 \text{ fA/cm}^2$ for n-type and of $4.5 \pm 2.2 \text{ fA/cm}^2$ on p-type substrates were obtained. The PCs prepared by photolithography will provide a valuable benchmark for this future work.

CRedit authorship contribution statement

J. Krügener: Conceptualization, Methodology, simulation, Formal analysis, AFM analysis, Writing – review & editing, Writing – original draft, preparation, and reviewing. **M. Rienäcker:** Conceptualization, lifetime characterization. **S. Schäfer:** Simulation, Writing – review & editing. **M. Sanchez:** Optical characterization. **S. Wolter:** Writing – original draft, preparation and, Writing – review & editing. **R. Brendel:** Writing – original draft, preparation and, Writing – review & editing. **S. John:** Investigation, Writing – review & editing. **H.J. Osten:** Supervision. **R. Peibst:** Writing – original draft, preparation, and, Writing – review & editing.

Declaration of competing interest

The authors declare that they have no known competing financial interests or personal relationships that could have appeared to influence the work reported in this paper.

Acknowledgements

We would like to thank H. Fischer, S. Spätlich, R. Winter, A. Raugewitz, G. Glowatzki and R. Zieseniß for sample processing, M. Wolf, A. Dietrich, R. Reineke-Koch for discussion and support with the measurement systems, and Sajeev John for fruitful discussions. This work is funded by the German Ministry for Economic Affairs and Energy (grant FKZ 003EE1056A) and the federal state of Lower Saxony.

References

- [1] B.A. Veith-Wolf, S. Schäfer, R. Brendel, J. Schmidt, Reassessment of intrinsic lifetime limit in n-type crystalline silicon and implication on maximum solar cell efficiency, *Sol. Energy Mater. Sol. Cell.* 186 (2018) 194–199, <https://doi.org/10.1016/j.solmat.2018.06.029>.
- [2] A. Richter, M. Hermle, S.W. Glunz, Reassessment of the limiting efficiency for crystalline silicon solar cells, *IEEE J. Photovoltaics* 3 (2013) 1184–1191, <https://doi.org/10.1109/JPHOTOV.2013.2270351>.
- [3] S. Schäfer, R. Brendel, Accurate calculation of the absorptance enhances efficiency limit of crystalline silicon solar cells with lambertian light trapping, *IEEE J. Photovoltaics* 8 (2018) 1156–1158, <https://doi.org/10.1109/JPHOTOV.2018.2824024>.
- [4] M. Green, E. Dunlop, J. Hohl-Ebinger, M. Yoshita, N. Kopidakis, X. Hao, Solar cell efficiency tables (version 57), *Prog. Photovoltaics Res. Appl.* 29 (2021) 3–15, <https://doi.org/10.1002/ppp.3371>.
- [5] F. Haase, C. Hollemann, S. Schäfer, A. Merkle, M. Rienäcker, J. Krügener, R. Brendel, R. Peibst, Laser contact openings for local poly-Si-metal contacts enabling 26.1%-efficient POLO-IBC solar cells, *Sol. Energy Mater. Sol. Cell.* 186 (2018) 184–193, <https://doi.org/10.1016/j.solmat.2018.06.020>.
- [6] S. Bhattacharya, S. John, Designing high-efficiency thin silicon solar cells using parabolic-pore photonic crystals, *Phys. Rev. Applied* 9 (2018), <https://doi.org/10.1103/PhysRevApplied.9.044009>.
- [7] J. Zhao, A. Wang, P. Altermatt, S. Wenham, M. Green, 24% efficient per silicon solar cell: recent improvements in high efficiency silicon cell research, *Sol. Energy Mater. Sol. Cell.* 41–42 (1996) 87–99, [https://doi.org/10.1016/0927-0248\(95\)00117-4](https://doi.org/10.1016/0927-0248(95)00117-4).
- [8] J. Zhao, A. Wang, M.A. Green, 24.5% Efficiency silicon PERT cells on MCZ substrates and 24.7% efficiency PERL cells on FZ substrates, *Prog. Photovoltaics Res. Appl.* 7 (1999) 471–474, [https://doi.org/10.1002/\(SICI\)1099-159X\(199911/12\)7:6<471::AID-PIP298>3.0.CO;2-7](https://doi.org/10.1002/(SICI)1099-159X(199911/12)7:6<471::AID-PIP298>3.0.CO;2-7).
- [9] P. Campbell, M.A. Green, High performance light trapping textures for monocrystalline silicon solar cells, *Sol. Energy Mater. Sol. Cell.* 65 (2001) 369–375, [https://doi.org/10.1016/S0927-0248\(00\)00115-X](https://doi.org/10.1016/S0927-0248(00)00115-X).
- [10] A. Chutinan, S. John, Light trapping and absorption optimization in certain thin-film photonic crystal architectures, *Phys. Rev. A* 78 (2008), <https://doi.org/10.1103/PhysRevA.78.023825>.
- [11] S. Kinoshita, S. Yoshioka, Structural colors in nature: the role of regularity and irregularity in the structure, *ChemPhysChem* 6 (2005) 1442–1459, <https://doi.org/10.1002/cphc.200500007>.
- [12] S. Kinoshita, S. Yoshioka, J. Miyazaki, Physics of structural colors, *Rep. Prog. Phys.* 71 (2008) 76401, <https://doi.org/10.1088/0034-4885/71/7/076401>.
- [13] E. Yablonovitch, Inhibited spontaneous emission in solid-state physics and electronics, *Phys. Rev. Lett.* 58 (1987) 2059–2062, <https://doi.org/10.1103/PhysRevLett.58.2059>.
- [14] S. John, Strong localization of photons in certain disordered dielectric superlattices, *Phys. Rev. Lett.* 58 (1987) 2486–2489, <https://doi.org/10.1103/PhysRevLett.58.2486>.
- [15] M.-L. Hsieh, A. Kaiser, S. Bhattacharya, S. John, S.-Y. Lin, Experimental demonstration of broadband solar absorption beyond the lambertian limit in certain thin silicon photonic crystals, *Sci. Rep.* 10 (2020) 11857, <https://doi.org/10.1038/s41598-020-68704-w>.
- [16] E. Yablonovitch, Statistical ray optics, *J. Opt. Soc. Am.* 72 (1982) 899, <https://doi.org/10.1364/JOSA.72.000899>.
- [17] S. Bhattacharya, S. John, Beyond 30% conversion efficiency in silicon solar cells: a numerical demonstration, *Sci. Rep.* 9 (2019) 12482, <https://doi.org/10.1038/s41598-019-48981-w>.
- [18] O. Tabata, R. Asahi, H. Funabashi, K. Shimaoka, S. Sugiyama, Anisotropic etching of silicon in TMAH solutions, *Sensor Actuator Phys.* 34 (1992) 51–57, [https://doi.org/10.1016/0924-4247\(92\)80139-T](https://doi.org/10.1016/0924-4247(92)80139-T).
- [19] J. Thong, W.K. Choi, C.W. Chong, TMAH etching of silicon and the interaction of etching parameters, *Sensor Actuator Phys.* 63 (1997) 243–249, [https://doi.org/10.1016/S0924-4247\(97\)80511-0](https://doi.org/10.1016/S0924-4247(97)80511-0).
- [20] P.-H. Chen, H.-Y. Peng, C.-M. Hsieh, M.K. Chyu, The characteristic behavior of TMAH water solution for anisotropic etching on both Silicon substrate and SiO₂ layer, *Sensor Actuator Phys.* 93 (2001) 132–137, [https://doi.org/10.1016/S0924-4247\(01\)00639-2](https://doi.org/10.1016/S0924-4247(01)00639-2).
- [21] S.A. Nadi, A. Gad, F. Lentz, Y. Augarten, K. Bittkau, A. Lambert, D.Y. Kim, L. Ding, A. Wrigley, U. Rau, K. Ding, Efficient light trapping in silicon heterojunction solar cells via nanoimprint periodic texturing, in: *IEEE 7th World Conference on Photovoltaic Energy Conversion (WCPEC) (A Joint Conference of 45th IEEE PVSC, 28th PVSEC & 34th EU PVSEC)*, IEEE, 2018, pp. 3062–3064, 62018.
- [22] S. Sivasubramaniam, M.M. Alkai, Inverted nanopyramid texturing for silicon solar cells using interference lithography, *Microelectron. Eng.* 119 (2014) 146–150, <https://doi.org/10.1016/j.mee.2014.04.004>.
- [23] C. Hollemann, F. Haase, M. Rienäcker, V. Barnscheidt, J. Krügener, N. Folchert, R. Brendel, S. Richter, S. Großer, E. Sauter, J. Hübner, M. Oestreich, R. Peibst, Separating the two polarities of the POLO contacts of an 26.1%-efficient IBC solar cell, *Sci. Rep.* 10 (2020) 658, <https://doi.org/10.1038/s41598-019-57310-0>.
- [24] F. Haase, F. Kiefer, S. Schäfer, C. Kruse, J. Krügener, R. Brendel, R. Peibst, Interdigitated back contact solar cells with polycrystalline silicon on oxide passivating contacts for both polarities, *Jpn. J. Appl. Phys.* 56 (2017), 08MB15, <https://doi.org/10.7567/JJAP.56.08MB15>.
- [25] K. Ramspeck, K. Bothe, J. Schmidt, R. Brendel, Combined dynamic and steady-state infrared camera based carrier lifetime imaging of silicon wafers, *J. Appl. Phys.* 106 (2009) 114506, <https://doi.org/10.1063/1.3261733>.
- [26] J. Muller, H. Hannebauer, C. Mader, F. Haase, K. Bothe, Dynamic infrared lifetime mapping for the measurement of the saturation current density of highly doped regions in silicon, *IEEE J. Photovoltaics* 4 (2014) 540–548, <https://doi.org/10.1109/JPHOTOV.2013.2293062>.
- [27] D.E. Kane, R.M. Swanson (Eds.), *Measurement of the Emitter Saturation Current by a Contactless Photoconductivity Decay Method*, 1985.